A hybrid framework for brain tissue segmentation in magnetic resonance images

Li, C., Sun, J., Liu, L. & Palade, V.

A hybrid framework for brain tissue segmentation in magnetic resonance images

Chao Li[1], Jun Sun*[1], Li Liu*[2], Vasile Palade[3]

Address: [1] Department of Computer Science and Technology, Jiangnan University, No.1800, Lihu Avenue, Wuxi, Jiangsu, 214122, China, [2] Big Data Center, Affiliated Hospital of Jiangnan University, No.1000, Hefeng Road, Wuxi, Jiangsu, 214000, China, [3] Centre for Data Science, Coventry University, Priory Street, CV1 5FB, Coventry, UK

E-mail: Chao Li - lcmeteor@hotmail.com; Jun Sun* - junsun@jiangnan.edu.cn; Li Liu* - 752295960@qq.com; Vasile Palade - ab5839@coventry.ac.uk;

*Corresponding authors

Abstract: Having a robust image segmentation strategy is very important in magnetic resonance image (MRI) processing for an effective and early disease detection and diagnosis. Since magnetic resonance images can present tissues of interest in both morphological and functional images, various segmentation techniques have been employed for this. The algorithms based on Markov Random Field (MRF) have shown strong abilities in dealing with noisy image segmentation compared to other methods. In this paper, inspired by the random drift particle swarm optimization (RDPSO) algorithm, we propose a novel hybrid framework based on a combination of the RDPSO with the Hidden Markov Random Field model and the Expectation-Maximization algorithm (HMRF-EM), to be used for MRI segmentation in real-time environments. The proposed hybrid framework is compared with the standalone HMRF-EM method, two other MRF-based stochastic relaxation algorithms, and two widely used brain tissue segmentation toolboxes on both simulated and real MRI datasets. The experimental results prove that

the proposed hybrid framework can obtain better segmentation results than most of its competitors and has faster convergence speed than the compared stochastic optimization algorithms.

Keywords: Brain tissue segmentation; Expectation-maximization; Hidden Markov Random Field; Magnetic Resonance Image; Random Drift Particle Swarm Optimization

1. Introduction

Segmentation of the brain magnetic resonance images (MRIs) is of fundamental importance in the analysis of brain tissues, and it is a challenging task for radiologists [1]. Many neurological diseases of brain are followed by subtle abnormal changes as shown in pathological studies [2]. MRI segmentation aims at partitioning brain images into regions so that each region groups contiguous voxels sharing similar attributes (intensity, luminance, etc.) [3]. The fundamental task of the 3D brain MRI segmentation involves the classification of the voxels into three primary tissue types: white matter (WM), gray matter (GM), and cerebrospinal fluid (CSF). This tissue classification has been the subject of intensive medical research for the last two decades, in which both supervised and unsupervised segmentation methods have been used [4, 5]. For example, supervised methods for MRI segmentation include support vector machines [6] and K-nearest neighbors [7, 8], and unsupervised methods include adaptive Markov modeling for mutual-information-based [9], K-means clustering or fuzzy c-means clustering [10, 11, 12]. Some semi-automatic methods have also been employed in this task [13, 14].

Among all the segmentation methods for MRI, the Markov random field (MRF) has been regarded as one robust and efficient methodology, which has been widely used in

computer vision [15] in dealing with image segmentation [12, 16], surface reconstruction [17] and other tasks [18, 19]. This method treats image segmentation as a labeling problem in order to find one optimal value of energy in the large solution space. Characterized as one universal model whose spatial information is encoded through contextual constraints of neighboring sites, MRFs can search the feasible space to get the optimum solution. Both the deterministic and stochastic optimization methods can be used to optimize the MRF model. However, the deterministic relaxation method, like the Iterated Conditional Modes (ICM) [20], heavily relies on initialization and may get trapped into local minima easily. By contrast, the stochastic relaxation method, such as Simulated Annealing (SA) [21], is more likely to get to a global minimum [22], while accompanied by heavy computational load.

Therefore, in order to solve these potential problems, many researchers have proposed novel methods or modified existing approaches for optimizing the MRF model employed in brain MRI segmentation [23]. For example, Tohka et al. [24] introduced a framework in which local models for tissue intensities and MRF priors were combined into a global probabilistic image model. Cardoso et al. [25] proposed a locally varying MRF-based model for enhancement of sulci and gyri. Yousefi et al. [26] presented a novel method based on MRF and a hybrid of an ant colony optimization and a Gossiping algorithm which can help find a better path using neighborhood information. In [27], Park et al. proposed a new segmentation method based on a hierarchical MRF model. The hierarchical MRF consists of local-level MRFs based on adaptive local priors and a global-level MRF that enhances the consistency of the local-level ones. In conclusion,

all of the aforementioned optimization methods could be divided into two groups, namely global methods and local ones. However, due to the algorithm limitations and the complicated neuroanatomical structure of the brain, many of these methods are still prone to get trapped into local minima when solving the brain MRI segmentation problems, and their segmentation efficiency can also be further improved.

In order to design an approach to solve brain MRI segmentation problems with high effectiveness and high efficiency, we propose a novel hybrid framework in this paper. On one hand, the random drift particle swarm optimization (RDPSO) algorithm [28] is first utilized to optimize the MRF model (RDPSO-MRF) in this framework. As a variant of particle swarm optimization (PSO) [29, 30], the RDPSO also shows better efficiency in solving many optimization tasks than many other stochastic optimization algorithms [28]. However, unlike the PSO, which has been proven to be neither a globally convergent nor a locally convergent algorithm [31], the sampling strategy of the RDPSO makes the algorithm have global convergence [28]. Therefore, in combination with the MRF model, the RDPSO can solve brain MRI segmentation problems with higher effectiveness and efficiency. On the other hand, to further improve the segmentation accuracy and convergence rate of the proposed hybrid framework, the HMRF-EM method, which can be easily combined with other stochastic techniques [32, 33, 34], is also employed in this work. As one variant of MRF, the Hidden Markov random field (HMRF) approach derives from hidden Markov model [32], and generally utilizes the expectation-maximization (EM) algorithm to complete its parameter estimation step [35].

In the proposed hybrid framework, the RDPSO-MRF algorithm is employed as a

global search technique to find potential candidates, while the HMRF-EM method is used as a local optimization method to further optimize the current best solution found by the RDPSO-MRF in some iterations. The cooperation between these two methods can make the hybrid framework obtain good segmentation accuracy within acceptable computational time. In order to verify the performance of our hybrid framework, we compared the proposed segmentation approach with the standalone HMRF-EM method, some variants of MRF model, and two widely used brain segmentation toolboxes on simulated data as well as real MRI dataset. The experimental results clearly demonstrate that our proposed method is superior to all the other compared methods in terms of segmentation accuracy in most cases, and is also much less time-consuming than the compared stochastic relaxation algorithms.

The organization of this paper is as follows. Section 2 describes the proposed hybrid framework for brain MRI segmentation. In Section 3, we present experimental validation of the proposed framework on both simulated and real datasets, by comparing it to other competitive brain tissue segmentation methods. Section 4 provides some conclusion and final remarks on this work.

2. Segmentation methodology

2.1 MRF theory and the HMRF-EM model

The MRF was first proposed in image analysis by Geman and Geman [36]. MRF is a stochastic process that models spatial coherence constraints within a labeling process through a neighboring system. In MRF, we consider two random fields for X and Y, as

detailed below. Suppose $\Omega = \{(i,j); 1 \leq i \leq M, 1 \leq j \leq N\}$ defines a two dimensional $M \times N$ lattice indexed by (i,j). On this lattice, let $Y = \{Y_s = y_s; s \in \Omega\}$ be the observation field and $X = \{X_s = x_s; s \in \Omega\}$ designate the label field which has values from $\varrho = \{0, 1, 2, \cdots, K - 1\}$, where K is the number of classes. Each site on Ω relates with another via a neighborhood system, which is defined as $N = \{N_s, s \in \Omega\}$, where N_s is the set of sites neighboring s that meet the condition $s \notin N_s$ and $s \in N_w \Leftrightarrow w \in N_s$. The label field X is said to be an MRF on Ω with regard to the neighborhood system N_s if and only if two below conditions are satisfied [37]:

$$P(x) > 0, \forall x \in X \tag{1}$$

$$P(x_s | x_{\Omega - \{s\}}) = P(x_s | x_{N_s}), s \in \Omega \tag{2}$$

According to the Hemmersley-Clifford theorem [38] and commonly used maximum a posteriori probability (MAP) criterion, the MRF problem is equal to minimizing the posterior energy $U(x)$ below

$$x^* = \arg\min_{x \in X}[U(x)] = \arg\min_{x \in X}[E(x) + \frac{(y - \mu)^2}{2\sigma^2} + \log(\sigma)] \tag{3}$$

A common probabilistic model used in Eq. (3) is the Gaussian distribution with mean μ and standard deviation σ. Since a specific brain tissue with common properties makes up one class, it is reasonable to suppose that the image values are distributed around the mean value of the class [39].

Eq. (3) is a nonconvex function, which means we should seek the global optimum in the entire solution space, and it clearly presents a computationally infeasible problem. Therefore, the stochastic relaxation algorithm is usually used to find the MAP estimation.

In [36], the SA algorithm employing the Metropolis sampling method was applied to solve this problem, and such an implementation is called the classical MRF (CMRF) model in this paper. The detailed description of the CMRF model could be found in the literature [15, 26, 40].

As a variant of the MRF model, the HMRF model is defined with respect to a pair of random variable families (X, Y), while the MRF is only defined on X [32]. By supposing that (X, Y) is pairwise independent and given the neighborhood configuration X_{n_s} of X_s, we can get the general form of Gaussian Hidden Markov Random Field model, that is

$$P\left(y_s \middle| x_{n_s}, \theta\right) = \sum_{l \in L} g(y_s, \theta_l) P(l | x_{n_s}) \tag{4}$$

where $\theta = \{\theta_l, l \in L\}$, L is the state space of X and $g(y_s, \theta_l)$ is the Gaussian probability density function.

Generally, the Expectation-Maximization (EM) algorithm is used to fit the HMRF model and estimate the parameter set $\theta_l = (\mu_l, \sigma_l)$. The EM algorithm is a method of parameter estimation from a given data set that is incomplete [41]. The main steps of the HMRF-EM framework could be found in [32].

2.2 Random drift particle swarm optimization

In this paper, the RDPSO algorithm was utilized to optimize the MRF model. The RDPSO algorithm is a probabilistic PSO variant and is first combined in this paper with the MRF model to deal with the MRI segmentation problems. In the canonical PSO with M particles, each particle i is regarded as a potential solution for a problem in a D-

dimensional space and denoted by its position $X_i^t = [X_{i,1}^t, X_{i,2}^t, \cdots, X_{i,D}^t]$ and its velocity

$V_i^t = [V_{i,1}^t, V_{i,2}^t, \cdots, V_{i,D}^t]$ at the tth iteration. At the $(t+1)$th iteration, the velocity and

position of particle i are updated according to the following two equations:

$$V_{i,j}^{t+1} = \omega V_{i,j}^t + c_1 rand_1^t \left(P_{i,j}^t - X_{i,j}^t \right) + c_2 rand_2^t \left(G_j^t - X_{i,j}^t \right) \tag{5}$$

$$X_{i,j}^{t+1} = X_{i,j}^t + V_{i,j}^{t+1} \tag{6}$$

where ω is the inertia weight, which can be adjusted to balance the exploration and

exploitation ability of each particle [30]. In the canonical PSO, ω is generally set to

linearly decrease from 0.9 to 0.4 according to the number of iterations. c_1 and c_2 are

known as the acceleration coefficients which control the influence of the social and

cognitive components. $rand_1$ and $rand_2$ are the sequences of two different random

numbers with uniform distribution on the interval $(0, 1)$. Generally speaking, the value

of $V_{i,j}^t$ is restricted within the interval $[-V_{max}, V_{max}]$. The vector $P_i^t = [P_{i,1}^t, P_{i,2}^t, \cdots, P_{i,D}^t]$ records the historical best position found by particle i, called the

personal best ($pbest$) position, and the vector $G^t = [G_1^t, G_2^t, \cdots, G_D^t]$ is the best position

among all the $pbest$ positions in the population and is called the global best ($gbest$)

position. Each $pbest$ position is updated by comparing the fitness values of the

particle's current position and its own $pbest$ position [42, 43].

According to the analysis of the particles' trajectory and the stability of the PSO

algorithm in [44], the canonical PSO may converge if each particle converges to its local

focus $p_i^t = (p_{i,1}^t, p_{i,2}^t, \cdots, p_{i,D}^t)$, which is defined at the following coordinates:

$$p_{i,j}^t = \frac{c_1 r_{i,j}^t P_{i,j}^t + c_2 R_{i,j}^t G_j^t}{c_1 r_{i,j}^t + c_2 R_{i,j}^t} \tag{7}$$

or

$$p_{i,j}^t = \varphi_{i,j}^t P_{i,j}^t + \left(1 - \varphi_{i,j}^t\right) G_j^t, \qquad \varphi_{i,j}^t \sim U(0,1) \tag{8}$$

Based on this the trajectory analysis of the canonical PSO, and motivated by the free electron in model metal conductors placed in an external electric field in [45], Sun et al. [28] proposed the RDPSO algorithm. Compared with the canonical PSO algorithm, the RDPSO generally have stronger global search ability and is less prone to be trapped into local optimal or suboptimal points. The velocity's sampling strategy of RDPSO differs from that of the canonical PSO significantly, which can be expressed as

$$V_{i,j}^{t+1} = \alpha |C_j^t - X_{i,j}^t| \phi_{i,j}^t + \beta (p_{i,j}^t - X_{i,j}^t) \tag{9}$$

where $C^t = (C_1^t, C_2^t, \cdots, C_D^t)$ is the mean best position ($mbest$), defined by the mean value of the $pbest$ of all M particles. The parameter α is called the thermal coefficient and β is called the drift coefficient. $\phi_{i,j}^t$ can be calculated by using the following equations:

$$\phi_{i,j}^t = \begin{cases} +\ln(1/u_{i,j}^t), & s > 0.5 \\ -\ln(1/u_{i,j}^t), & s \leq 0.5 \end{cases} \tag{10}$$

where s and $u_{i,j}^t$ are two different random numbers uniformly distributed on $(0,1)$. The thermal and drift coefficients (α and β) are the most important algorithmic parameters in the RDPSO algorithm. In [28], it was recommended that for the RDPSO, α should be set to be no larger than 1.0 and β to be no larger than 1.5. In our experiment, in order to obtain good brain MRI segmentation results, the value of α is set to linearly

decrease from 1.0 to 0.5 according to the iteration number t, and the value of β is fixed to 1.0. The detailed derivation process of Eq. (9) and the corresponding analysis of the RDPSO algorithm can be found in the [28].

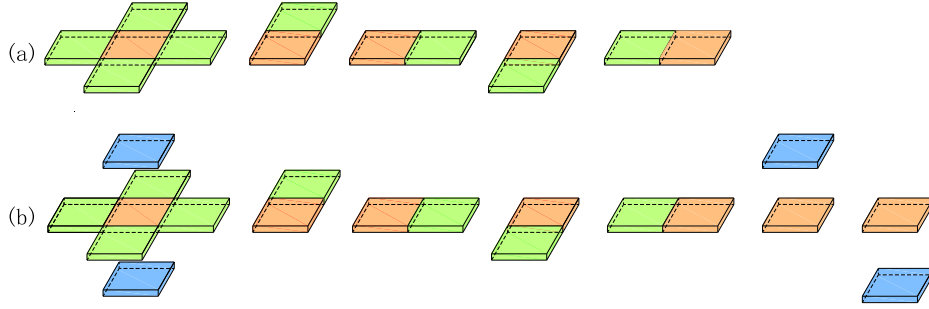## 2.3 The energy function and the fitness function

Fig.1 The illustration of the neighborhood system, left to right: label fields, clique of orange filled site. (a) the 2D first order neighborhood with 4 neighbors; (b) the 3D first order neighborhood with 6 neighbors.

In this work, we draw on the information of three sequenced slices from brain MRI data. Therefore, in order to guarantee the validity of the followed experiments, all of the MRF-based methods introduced in this paper, including our proposed algorithm and other compared algorithms, utilize the same three-dimensional neighborhood system as shown in Fig.1(b). The prior model defined by the $3D$ first order neighborhood has 6 neighbors, which is distinct from that of the original MRF model in a two-dimensional lattice as described in Fig.1(a).

Due to the possibility of anisotropic voxel size and slice spacing, the interaction between neighbors in each direction should be different. However, considering the computational efficiency, we assume that the interaction between a voxel and its neighbors in the x direction is the same as that in y direction, but is different from that in the z direction. Therefore, a simplified prior model [24, 25, 46] is used to compute the energy function in this paper, which is defined by:

$$E(x) = \beta \left(\sum_{j \in N_i^{xy}} \frac{G_{ij}}{d(s_i, s_j)} + \sum_{z \in N_i^{z}} \frac{H_{iz}}{d(s_i, s_z)} \right) \tag{11}$$

where $d(,)$ is the Euclidean distance between the centers of two voxels; β is a user tunable regularization parameter that is meant for the overall strength of the interaction between pair-wise neighboring voxels, controlling the tradeoff between the prior model and the likelihood; $N_i = \{N_i^{xy}, N_i^{z}\} = \{\{i^n, i^s, i^w, i^e\}, \{i^t, i^b\}\}$ defines the 3D MRF neighborhood system, where i^n, i^s, i^w and i^e are its four neighbors in the plane, and, i^t and i^b are its two neighbors out of the plane; G and H are $K \times K$ energy matrices that together form the MRF parameters $\Phi = (G, H)$, where K is number of tissue types. Instead of estimating and updating G and H at each iteration, we assume constant values based on anatomical proprieties of the brain, that is

$$G_{ij} = \begin{cases} 0, & \text{class } i \text{ is the same as } j \\ \alpha, & \text{class } i \text{ is next to } j \\ \gamma, & \text{class } i \text{ is far from } j \end{cases} \tag{12}$$

$$H_{iz} = \begin{cases} 0, & \text{class } i \text{ is the same as } z \\ R_f, & \text{class } i \text{ is next to } z \\ 0, & \text{class } i \text{ is far from } z \end{cases} \tag{13}$$

with $0 \leq \alpha \leq \gamma$ and $0 \leq R_f \leq 1$ [25]. α and R_f are penalty factors for

anatomically neighboring classes, and γ is a penalty factor for anatomically distant classes. A larger γ could lead to a lower probability for two voxels with anatomically distant labels to be together. A larger α would increase the sharpness of the transitions between neighboring tissue, leading to more robust but less sensitive segmentation. The values of α, γ and R_f used in this paper are 0.5, 3 and 0.3, respectively.

In this paper, since we incorporate the RDPSO algorithm into the MRF-MAP framework, the estimation of the MAP problem represented by Eq. (3) is converted to the optimization of the fitness function by RDPSO. By integrating the above energy function $E(x)$ with the MRF-MAP framework, the fitness function used in our work can be obtained ultimately as:

$$U(x) = \arg \min_{x \in X}[\beta \left(\sum_{j \in N_i^{xy}} \frac{G_{ij}}{d(s_i, s_j)} + \sum_{z \in N_i^z} \frac{H_{iz}}{d(s_i, s_z)} \right) + \frac{(y - \mu)^2}{2\sigma^2} + \log(\sigma)] \quad (14)$$

where β is set to be 0.7 empirically. The first item is the energy of the prior model, and the last two items are the energy of the likelihood function that fits the Gaussian distribution. They constitute the objective function that we intend to optimize.

2.4 The proposed hybrid framework

In order to further improve the segmentation accuracy and accelerate the convergence speed for the brain MRI segmentation problem, we present a new hybrid framework comprising the RDPSO-MRF model and the well-known HMRF-EM algorithm (see section 2.1) to solve MRI segmentation problems. The RDPSO-MRF model utilizes the RDPSO algorithm to optimize the fitness function defined by the

MRF-MAP. During the search process of the RDPSO, the HMRF-EM scheme is used to further optimize the current best solution found by the RDPSO algorithm when some conditions are satisfied. Since the HMRF-EM has been proven to be powerful for segmentation of brain MRIs [32], the further optimization by the HMRF-EM can accelerate the convergence speed of the RDPSO and achieve better segmentation results. The pseudocode of the proposed approach is outlined in Algorithm 1, and the corresponding flowchart is illustrated in Fig.2. The specific setting of the corresponding parameters for the proposed hybrid framework can be found in Table 1.

Algorithm 1: The RDPSO-MRF&HMRF-EM framework

---

1 **begin**

2   Preprocess the input MRI;

3   Set M, K, $MAXITER$, N_{em}, N_s, N_u;

4   Initialize the current position $X_{i,j}^0$ $(1 \leq i \leq M, 1 \leq j \leq 2K)$;

5   Compute $U(X_i^0)$ and initialize $P_{i,j}^0$ of each particle, and then find G^0;

6   Set $N_c = 0$, $count = 0$;

7   **for** $t = 1$ **to** $MAXITER$ **do**

8   Update population X^{t-1} to X^t following Eqs. (8) and (5);

9   Compute $U(X_i^t)$ of each particle;

10   Update P_i^t of each particle and find G^t;

11   Update the current segmentation result seg^t represented by G^t;

12   **if** $U(G^t) == U(G^{t-1})$ **then**

13             $count = count + 1$;

14   **end if**

15   **if** $count \geq N_s$ **then**

16             $[pos_{EM}, seg_{EM}] = \text{HMRF\_EM}(G^t, seg^t, N_u)$;

17             $N_c = N_c + N_u$;

18	$count = 0$;
19	**if** $U(pos_{EM}) < U(G^t)$ **then**
20	$G^t = pos_{EM}$;
21	$U(G^t) = U(pos_{EM})$;
22	$seg^t = seg_{EM}$;
23	**else**
24	Break; /* The whole search process is terminated */
25	Output seg^t;
26	**end if**
27	**end if**
28	**end for**
29	**if** $N_c < N_{em}$
30	$[pos_{EM}, seg_{EM}] = HMRF\_EM(G^{MAXITER}, seg^{MAXITER}, N_{em} - N_c)$;
31	**if** $U(pos_{EM}) < U(G^{MAXITER})$
32	Output seg_{EM}; /* The whole search process is terminated */
33	**else**
34	Output $seg^{MAXITER}$; /* The whole search process is terminated */
35	**end if**
36	**else**
37	Output $seg^{MAXITER}$; /* The whole search process is terminated */
38	**end if**
39	**end**

As shown in Algorithm 1, after preprocessing the brain MRI data, M particles are initialized for the RDPSO-MRF model. Each particle represents a set including the $2K$ parameters, denoted by $\theta_{l_k \in L} = (\mu_1, \mu_2, \cdots, \mu_k; \sigma_1, \sigma_2, \cdots, \sigma_k)$, where $L = \{l_k; k = 1, 2, \cdots, K\}$ represents a set of tissue classes and K denotes the number of classes. Here we usually set K to be 4, considering that the main tissue classes in MRI are GM, WM, CSF, and background. The fitness value of each particle is measured by the

objective function (i.e. the fitness function) defined in Eq. (14). Then, the whole population with M particles is updated iteratively by following Eqs. (9) and (6). In each iteration, the $pbest$ position of each particle and the $gbest$ position should also be updated based on the comparison of fitness values. During the search process, once the $gbest$ position stops updating in consecutive N_s iterations, the HMRF-EM method was employed to further optimize the current $gbest$ position and thus accelerate the convergence speed. Using the current $gbest$ position G^t and current segmentation result seg^t obtained by the RDPSO as the two input arguments, the HMRF-EM method firstly carries out the MRF-MAP estimation to get the optimal class labels and total energy, and then uses the EM algorithm to iteratively optimize the parameters $\theta_{x_s} = (\mu_{x_s}, \sigma_{x_s})$ for N_u times, through transforming the input $gbest$ position G^t. If the HMRF-EM method successfully updates the fitness value of the $gbest$ position, the current $gbest$ position of the RDPSO algorithm is replaced to the better one and then the RDPSO algorithm continues to optimize the MRF model, and otherwise the whole search process of the hybrid framework is terminated. Besides, if the RDPSO algorithm reaches its maximum number of iterations $MAXITER$ while the HMRF-EM method does not reach its cumulative maximum number of iterations N_{em}, a continuous HMRF-EM search process with $N_{em} - N_c$ (N_c is the current cumulative number of iterations of the EM method) number of iterations should be implemented, since enough cumulative number of iterations of the HMRF-EM method can significantly enhance the robustness of the hybrid framework.
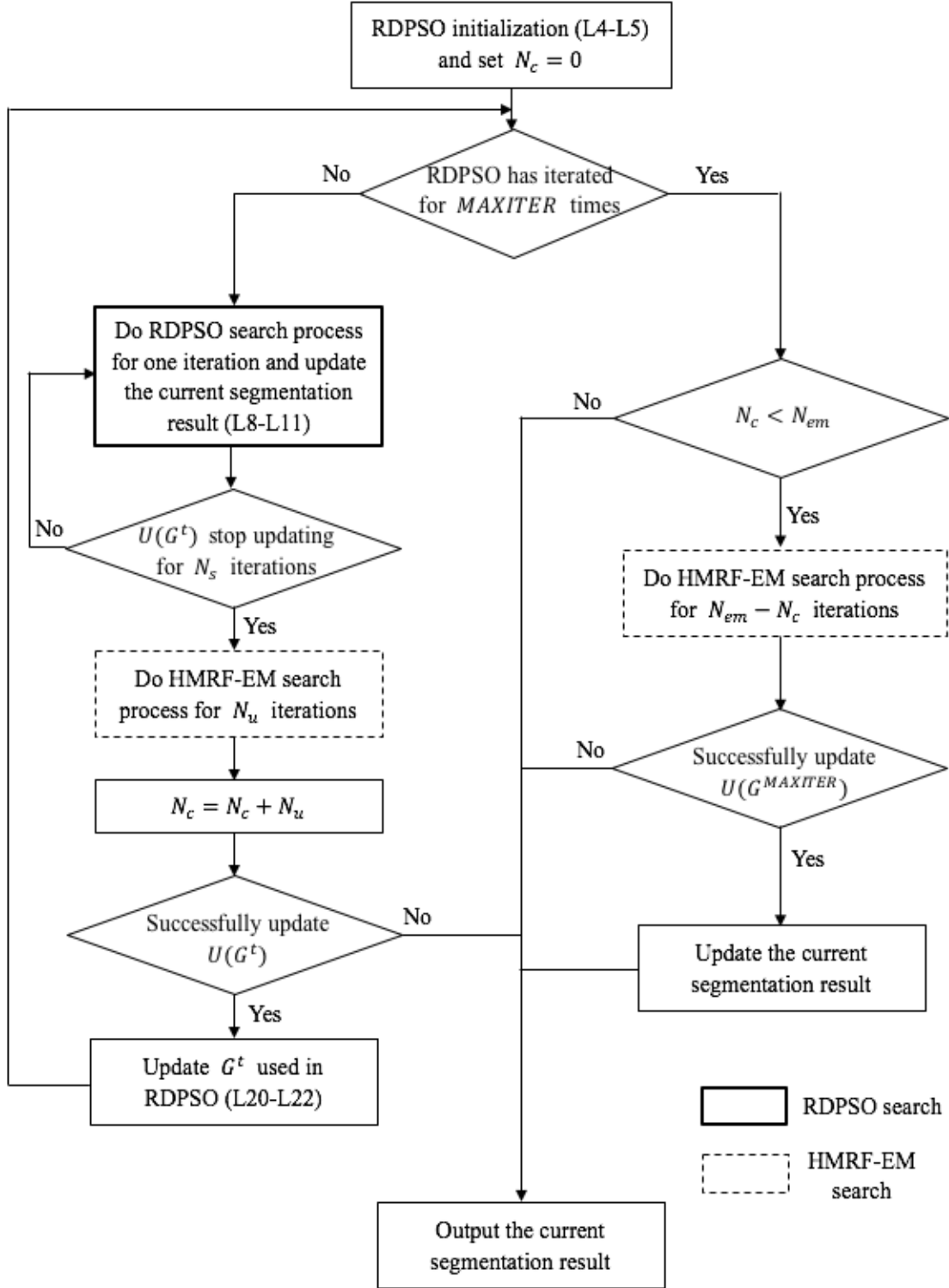
Fig.2 Flowchart of the proposed approach (L* represents the operation in the "* line" in Algorithm 1)

Therefore, the termination conditions in this hybrid algorithm can be divided into two types, as shown in Fig.2. One is obviously when the RDPSO and the HMRF-EM

have both reached their maximum number of iterations (line 32 and line 37 in Algorithm 1). The other is that if the HMRF-EM does not find a better solution than the current $U(G^t)$ within the specified number of iteration steps, the algorithm is regarded to have converged and should be terminated (line 24 and line 34 in Algorithm 1). The reason for the setting of the latter type is that in our preliminary experiments, we found that the HMRF-EM method can quickly update the current $gbest$ solution found by the RDPSO within a limited number of iterations. Therefore, if the energy value of the $gbest$ position found by the RDPSO cannot be updated by the HMRF-EM method within the specified number of iterations (N_c or $N_{em} - N_c$ iterations), the current $gbest$ solution can be regarded as the global optimal solution and the whole search process should be terminated.

With respect to the theoretical computational complexity, the computational costs of the proposed hybrid algorithm comprise that of the initialization (T_{ini}), the RDPSO operation (T_{RD}) and the HMRF-EM operation (T_{EM}). The T_{RD} involves the evaluation and the position update for each particle, and the T_{EM} contains the evaluation and the position update. Since there are several termination conditions in this algorithm, only the worst-case time complexity is analyzed here, that is, the time complexity when the hybrid algorithm completes the maximum iterations. For each particle, we assume T_{RD_ini} to be the time of initialization in the RDPSO, T_{RD_upd} the time of the velocity and position update in the RDPSO, T_{EM_upd} the time of the position update in the HMRF-EM, and T_{eva} the time of one fitness function evaluation. Therefore, the worst-case time complexity of the proposed algorithm can be calculated as $T = T_{ini} + (T_{RD} + T_{EM}) =$

$T_{\text{RD\_ini}} \cdot M + (T_{\text{RD\_upd}} + T_{\text{eva}}) \cdot M \cdot MAXITER + (T_{\text{EM\_upd}} + T_{\text{eva}}) \cdot N_{em} = M \cdot$

$T_{\text{RD\_ini}} + M \cdot MAXITER \cdot T_{\text{RD\_upd}} + N_{em} \cdot T_{\text{EM\_upd}} + (M \cdot MAXITER + N_{em}) \cdot T_{\text{eva}}$.

Since in this MRI segmentation problem, the time of the fitness function evaluation T_{eva} is generally much longer than $T_{\text{RD\_ini}}$, $T_{\text{RD\_upd}}$ and $T_{\text{EM\_upd}}$, Algorithm 1 has an $O(M \cdot MAXITER + N_{em})$ time complexity, associated with the number of particles and the iteration numbers of both the RDPSO and HMRF-EM operations.

Compared with the CMRF and its variants, the proposed hybrid framework adopts the HMRF-EM framework to accelerate the convergence and further improve the segmentation accuracy. Compared with the standalone HMRF-EM method, the proposed hybrid framework uses the current best solution obtained by the RDPSO as the initial solution for each HMRF-EM implementation, while the standalone HMRF-EM method generally adopts the K-means algorithm to produce the initial value. Undoubtedly, our current best solution generated by the RDPSO-MRF is much different from what the K-means does with respect to the overall segmentation performance, which may help the HMRF-EM method find better results within limited number of iterations for the EM algorithm.

3. Experimental results

In this section, in order to show the applicability of the proposed approach to the segmentation of MRIs of brain tissue as well as its robustness to noise, we tested our segmentation approach on simulated data as well as real MRI dataset.

3.1 Performance metrics

For the sake of quantitatively measuring the effectiveness and robustness of our proposed algorithm against the known ground truth, the following two segmentation similarity metrics are employed in our experimental analyses.

The Dice similarity coefficient (DSC) known as the mean and standard deviation of the Dice measure is used as the performance evaluation between the ground truth and the segmentation result. It is computed separately for each class (CSF, GM and WM). The DSC metric measures the degree of spatial overlap between two binary images and its value ranges from 0 and 1, which is defined as

$$\text{DSC}(U,V) = \frac{2|U \cap V|}{|U| + |V|} \tag{15}$$

where U is the segmentation result, V is the ground truth and $|\cdot|$ signifies the number of voxels contained in a set. The value of the $\text{DSC}(U,V)$ ranges from 0.0 to 1.0. The larger ultima value we get from DSC, the better segmentation result we achieve. However, the DSC metric has its own limitations in this application since it is sensitive to misplacement of the segmentation label and tends to attain higher values for larger structures than smaller ones [47]. One drawback of the DSC metric is that it is unsuitable for comparing segmentation accuracy on objects that differ in size [48]. So, it might not directly relate to an accuracy of clinical decisions.

Therefore, in this paper, we also adopt the commonly used miss-classification rate (MCR) performance to measure the overall segmentation quality, which is defined as:

$$\text{MCR} = \frac{\text{Number of miss classified voxels}}{\text{Total number of voxels}} \tag{16}$$

It is a kind of error measurements that are used to evaluate the overall segmentation result. It is also called "segment deletion" or "miss detection", referring to the failure of the

algorithm to classify actual labels. As can be seen, the smaller the MCR is, the more accurate segmentation result can be acquired.

3.2 Comparative methods and parameter settings

In order to evaluate the outperformance of our proposed method over other segmentation methods, our hybrid framework of RDPSO-MRF and HMRF-EM algorithms was compared with three MRF-based segmentation schemes and two other widely used brain tissue segmentation toolboxes.

With respect to the algorithms based on the MRF model, the first is the CMRF implementation described in section 2.1 that is used as a standard method in MRF classification and is based on a stochastic relaxation algorithm and Metropolis sampling method [36]. Since our proposed algorithm is also a global optimization method, it is reasonable to compare it with the CMRF model to demonstrate its performance. The termination condition of the CMRF implementation is when the local energy variation goes to zero. The second compared algorithm is the HMRF-EM method, which has also been described in section 2.1. As our proposed hybrid framework contains the HMRF-EM part, it makes sense to experiment on the standalone HMRF-EM framework to verify the superiority of our hybrid approach. The termination condition of the HMRF-EM framework is when the total energy of label field stops changing significantly ($|U(X^t) - U(X^{t-1})| < 10^{-3}$). The final MRF variant is the MRF implementation based on the canonical PSO algorithm introduced in section 2.2. As has been illustrated, the RDPSO algorithm, which is the core of our hybrid framework, is a variant of the PSO algorithm, and therefore it is valuable to compare the proposed framework with the

method where the PSO is used as a parameter optimizer. In the PSO-MRF method, the termination condition is that the optimization algorithm reaches the maximum number of iteration steps.

Two widely used toolboxes for brain tissue segmentation, i.e., the statistical parametric mapping (SPM) toolbox [49, 50, 51] and the partial volume classifier (PVC) [52, 53], were also used as competitive methods in the experiments. The SPM toolbox utilizes the parameter estimations of Gaussian mixer model (GMM) [49] for the brain tissue segmentation. In this study, the latest version of SPM (SPM12) was employed [54]. The PVC is implemented in the BrainSuite software. The brain tissue segmentation method for the PVC is based on the maximum-a-posteriori classifier and spatial prior model of the brain [52]. The version of the BrainSuite software adopted in this paper is BrainSuite18a [55], which corresponds to the version of Matlab used (see below).

The brain segmentation methods described above were all implemented in the Matlab programming environment (Matlab R2018a) running on an Intel 3.60 Giga-Hz CPU system with 128 Giga-Bytes memory. Except for the proposed framework, the parameter configurations of all the other compared algorithms are those recommended by the corresponding references. Since the CMRF, the PSO-MRF and the proposed method are stochastic relaxation algorithms, their mean value of the performance metrics (DSC and MCR) for each slice is the average result obtained after 30 runs, while HMRF-EM, SPM and PVC were run only one time, since their DSCs and MCRs on the same slice were invariant in different runs. The parameter configurations for each MRF-based method are listed in Table 1.

Table 1

Parameters of CMRF, HMRF-EM, PSO-MRF and RDPSO-MRF&HMRF-EM.

CMRF		HMRF-EM		PSO-MRF		RDPSO-MRF &HMRF-EM	
Parameters	Value	Parameters	Value	Parameters	Value	Parameters	Value
$T_{initial}$	4	N_{em}	50	M	40	M	40
$T_{multiple}$	0.97	N_{map}	10	ω	0.9→0.4	α	1.0→0.5
				$c_1 \& c_2$	2	β	1.0
				$MAXITER$	100	$MAXITER$	100
						N_{em}	50
						N_{map}	10
						N_s	5
						N_u	5

The parameters listed in Table 1 are explained as follows. $T_{initial}$: the initial temperature in SA, $T_{multiple}$: the temperature multiplier computed after traversing all the voxels, N_{em}: the total number of iterations of the EM algorithm, N_{map}: the number of iterations of the MAP process, M: the population size, ω: the inertia weight, $c_1 \& c_2$: the acceleration coefficients, $MAXITER$: the number of iterations in each run, α: the thermal coefficient, β: the drift coefficient, N_s: the maximum number of iterations for the RDPSO algorithm to continuously stop updating the fitness value of $gbest$, N_u: the number of iterations of the EM algorithm for each execution of the HMRF-EM method.

3.3 Simulated Data

The simulated 3D MRIs are provided by the BrainWeb simulated brain database from the McGill University [56]. The BrainWeb is a public dataset that offers realistic simulation of MRI acquisition with different levels of noise and inhomogeneities.

Simulated magnetic resonance phantoms are generated based on an anatomical model of the real brain. We selected the 3D simulated T1-weighted MRI data with 3% noise-level and 20% intensity non-uniformity (INU, also known as bias field) percentage. The data size is $181 \times 217 \times 181$ voxels of $1mm^3$ isotropic resolution. First, we performed some tasks to extract skull and scalp tissues. With the available ground truth from Brainweb, we used the ground truth of the brain mask to delineate the brain. Then, we could get the only four parts including CSF, WM, GM, and the background. Some methods reported in the literature have been employed to minimize the potential effects of the bias field in the next step, as a result of its bias effect on the accuracy of the final segmentation results [3] [9] [10] [25]. However, as our attention mainly focuses on the optimization of MRF by some stochastic algorithms, which is also accompanied by relatively heavy computational load, we directly employed our proposed method and the compared algorithms to segment the MRIs without further considering the bias field compensation.

Table 2

Mean DSC and mean MCR of all the slices obtained by all the compared methods on the BrainWeb dataset

Method	Mean DSC	Mean MCR
CMRF	0.821 ± 0.069	0.289 ± 0.059
PSO-MRF	0.810 ± 0.076	0.294 ± 0.086
HMRF-EM	0.822 ± 0.062	0.287 ± 0.044
SPM	0.826 ± 0.065	0.281 ± 0.086

|		
PVC	0.808 ± 0.084	0.313 ± 0.112
Proposed	0.845 ± 0.070	0.269 ± 0.057

In order to compare the MRI segmentation methods quantitatively on the BrainWeb dataset, we recorded in Table 2 the mean DSC and the mean MCR of all the slices obtained by all the compared methods. The mean performance metrics in Table 2 is the average value of DSC or MCR of three tissues (i.e., CSF, GM and WM) over all the slices in this dataset. It can be observed that in Table 2, for most of the evaluation criteria, the proposed hybrid algorithm is better than the other five methods, only except that the standard deviation of the mean DSC by the proposed method is a little larger than those obtained by the SPM, the PSO-MRF and the HMRF-EM, and the standard deviation of the mean MCR by the proposed method is just worse than that obtained by the HMRF-EM. Moreover, the advantages of the proposed algorithm over all the other compared methods on the evaluation criteria in terms of the mean values are significant. Therefore, it can be concluded that our proposed method had better performance than the three MRF-based methods as well as the other two brain tissue segmentation toolboxes from an overall perspective.
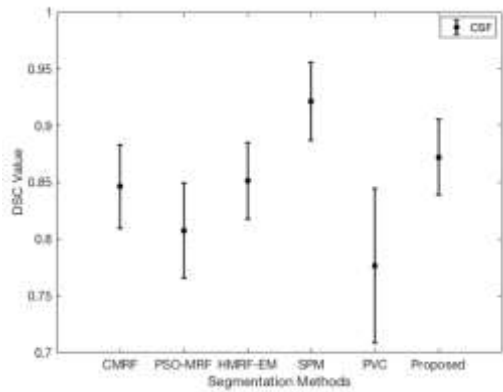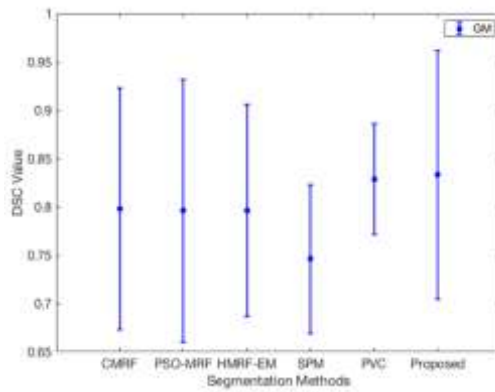
(a)   **(b)**
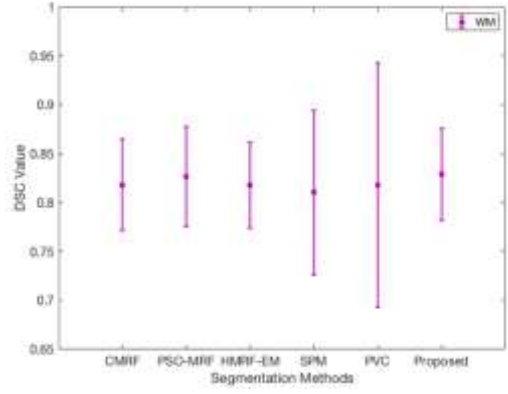
(c)

Fig.3 Mean DSC value obtained by each method on the BrainWeb dataset for (a) CSF (b) GM and (c) WM. The whiskers show plus/minus one standard deviation.

More specifically, in order to compare the segmentation accuracy on each tissue, we plot in Fig.3 the mean DSC values along with the standard deviations of all the slices corresponding to CSF, GM, and WM tissues for all the compared methods. From Fig.3, we can find that for each type of tissue, our hybrid framework produced better mean DSC value than most of the other competitive methods with only one exception, that the SPM is better than the proposed method for the average DSC on the CSF. The standard deviation of the proposed method on each tissue is also comparable to most of the other methods, especially for CSF and WM tissues, which shows the good robustness of the hybrid algorithm. It should be pointed out that benefiting from the proposed hybrid framework, the RDPSO-MRF&HMRF-EM algorithm shows its great advantage on the DSC values for the CSF and GM tissues over the other compared MRF-based methods, indicating the superiority of our proposed framework. An example of the segmentation results of a typical slice by the six compared methods together with the original slice and the ground truth are demonstrated in Fig.4.

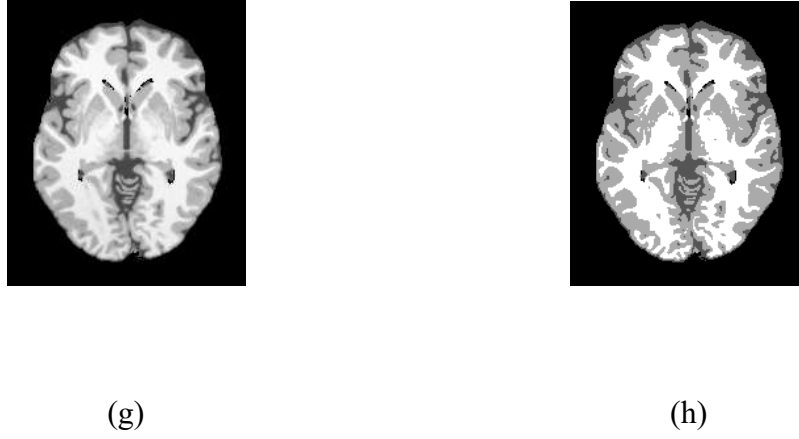(a)

(b)

(c)

(d)

(e)

(f)

<p align="center">(g)   (h)</p>
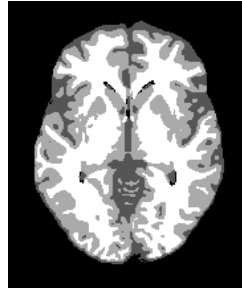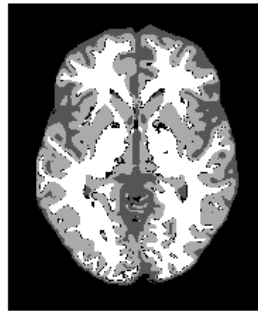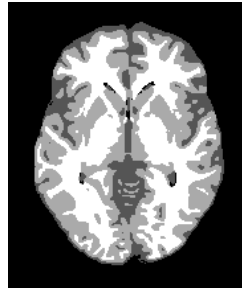
Fig.4 The segmentation results obtained by (a) CMRF, (b) PSO-MRF, (c) HMRF-EM, (d) SPM, (e) PVC, (f) the proposed method along with (g) the original slice and (h) the ground truth. Image: BrainWeb slice70 (WM in white, GM in light gray, CSF in dark gray and the background in black).
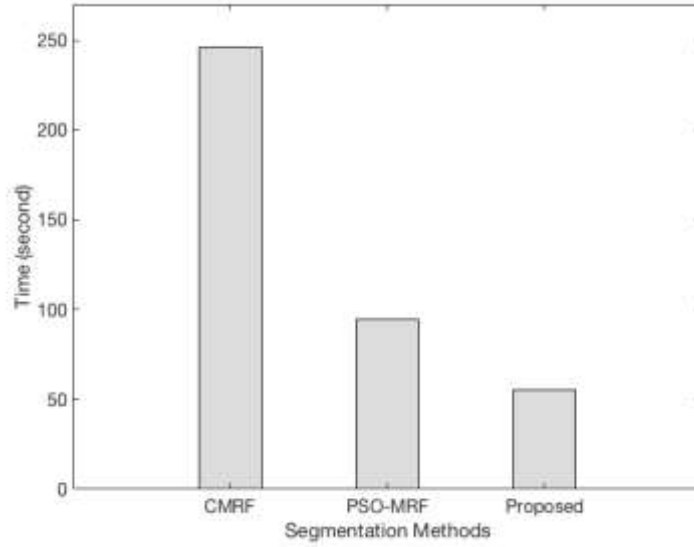

Fig.5 Comparison of the mean computational time over each slice by the CMRF, the PSO-MRF and the proposed method for the BrainWeb dataset.

Fig.5 shows the computational time by three methods in each round averaged on each slice for the BrainWeb dataset. It can be seen that the average value for our proposed method is 55.10s, while those for the CMRF and the PSO-MRF are 246.02s and 94.41s,

<p align="center">27</p>

respectively. Therefore, the average of computational time reduction percentages of the proposed method corresponding to the CMRF and the PSO-MRF method are significant, i.e., 77.60% and 41.64%, respectively, verifying that our proposed method is much less time-consuming than the other two stochastic relaxation algorithms. Here, we do not consider the computational time taken by the HMRF-EM, SPM and PVC due to their fast convergence rate based on local optimality, and thus only the time taken by the stochastic relaxation methods are compared. It should be noted that the time complexity of the PSO-MRF, which can be estimated as $O(M \cdot MAXITER)$, is actually lower than that of the proposed method (see section 2.4), but the mean computational time by the PSO-MRF is higher than that by the proposed method. The reason is that the computational time taken by the proposed method is less than that in the worst case in many cases, while the PSO-MRF always needs to evaluate the fitness function for $M \cdot MAXITER$ times. In other words, the carefully set termination conditions (see section 2.4) can make the proposed method take less computational time than the PSO-MRF in many cases.

In order to further illustrate the fast convergence speed during the search process and the effectiveness of the set termination conditions, we plotted in Fig.6 the convergence curves of the CMRF, the PSO-MRF and the proposed method for one run on the 70th slice (slice70) of the BrainWeb dataset as an example. Fig.6 illustrates that the fitness value of the proposed hybrid framework reduces much faster than the other two algorithms with respect to the number of fitness function evaluations. Fig.6 also clearly demonstrates that the implementation of the HMRF-EM method can significantly

accelerate the convergence speed (see the red line segments in Fig.6). Moreover, the number of iterations by the proposed method is much smaller than those by the other algorithms due to the carefully set termination conditions, which can also save much computational time.
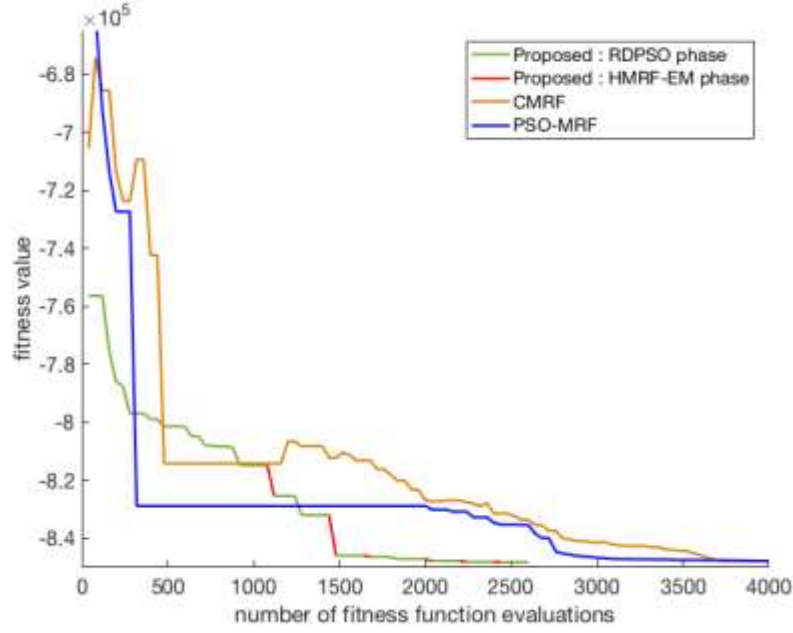

Fig.6 The convergence curves of the CMRF, the PSO-MRF and the proposed method for one run. Image: BrainWeb slice70.

3.4 Real datasets

This section shows validation results for real expert-classified MRIs, which were obtained from the Internet Brain Segmentation Repository (IBSR) [57]. The IBSR provides manually-guided expert segmentation results along with MRI data. In our experiments, we selected the IBSR_V2.0 (hereinafter referred to as IBSR2.0) dataset [58]. The IBSR2.0 dataset comprises 18 real T1-weighted MRI scans of normal subjects, named as IBSR_01 to IBSR_18. The data size of each subject is $256 \times 128 \times 256$ with voxels of size $0.94mm \times 1.5mm \times 0.94mm$. The ground truth for each subject in this

dataset can be downloaded from the IBSR repository. As the IBSR2.0 dataset contains in total 18 different MRI scan data, this segmentation task is more challenging for our proposed framework as well as the comparative methods.
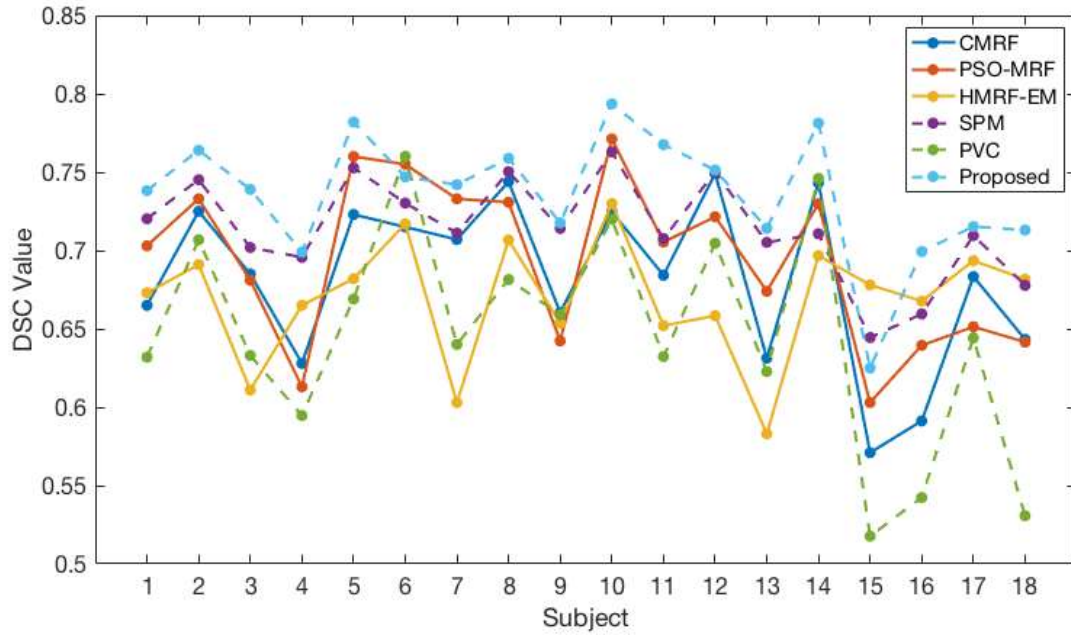

(a)
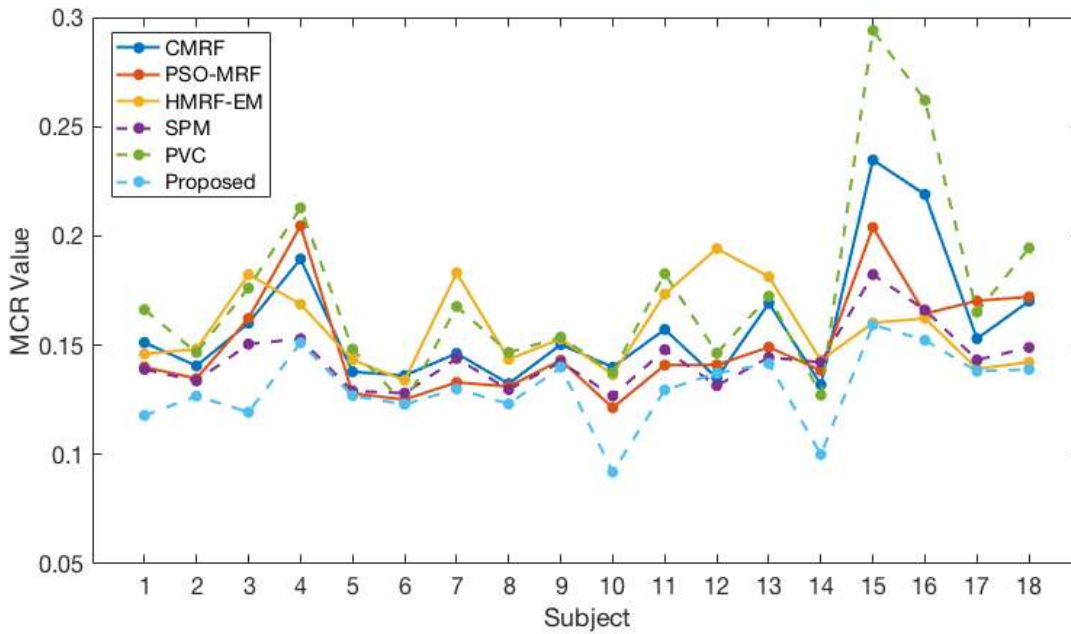
(b)

Fig.7 (a) The mean DSC and (b) the mean MCR over all the slices for each subject from
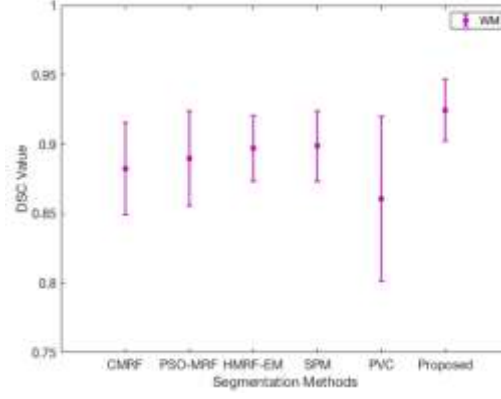
the IBSR2.0 dataset obtained by each method.

Fig.7 compares the average values of some evaluation criteria over all the slices for each subject from the IBSR2.0 dataset. From Fig.7, we can find that our hybrid framework produced overall better DSC value than the other competitive methods in most cases. The two exceptions are that the results of PSO-MRF and PVC are better than that of the proposed method for IBSR_06, and the results of HMRF-EM and SPM are better than that of the proposed method for IBSR_15. For the mean MCR obtained by each subject, our proposed method is also superior to the others only except that the result of SPM is better than that of the proposed method for IBSR_12. Nevertheless, for all the aforementioned subjects which the hybrid algorithm cannot obtain the best results, there is quite small difference between the results of the proposed method and those of the better ones. By comparison, for most of the other cases, the advantage of the RDPSO-MRF&HMRF-EM over the other compared methods is more obvious, which demonstrates the superiority of the proposed hybrid approach.


(a)   (b)

31
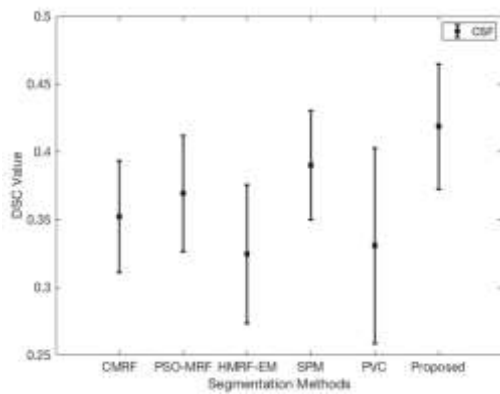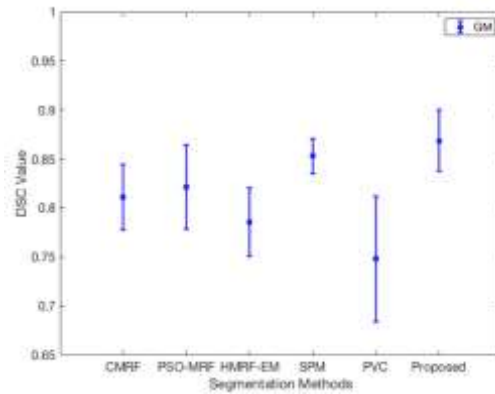
(c)

Fig.8 Mean DSC value obtained by each method over all the subjects of the IBSR2.0 dataset for (a) CSF (b) GM and (c) WM. The whiskers show plus/minus one standard deviation.

The mean DSC value obtained by each method for each kind of tissue over all the subjects of the IBSR2.0 dataset is presented in Fig.8. Comparing the results in Fig.8 and Fig.3, we can find that the advantage of the proposed method over the others on the real dataset is more remarkable than that on the simulated dataset, for the RDPSO-MRF&HMRF-EM method can get the highest mean DSC value for each kind of tissue in the IBSR2.0 dataset. Therefore, the proposed hybrid framework is maybe more suitable for real datasets than for the simulated ones. Furthermore, according to Fig.8, the standard deviations for the proposed method are comparable or better than those for the other methods in most cases, which demonstrates the good robustness of the hybrid method again. Therefore, it can be concluded that the segmentation accuracy of the proposed hybrid framework is better than those of the other compared methods for the IBSR2.0 dataset, and this is true in most cases. As an example, Fig.9 illustrates the segmentation results obtained by all the compared methods along with the original slice
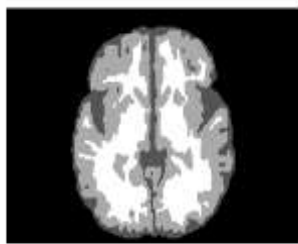
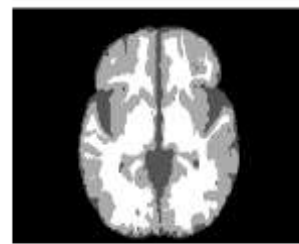and the ground truth for the 128th slice of the IBSR_01 subject in this dataset.
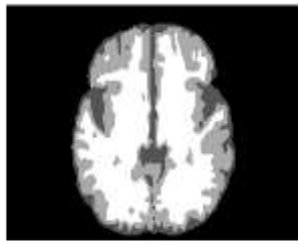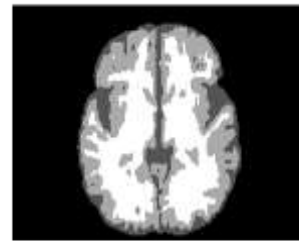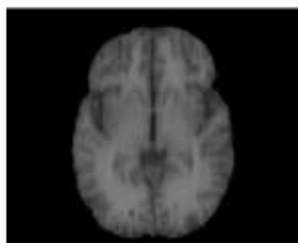

(a)
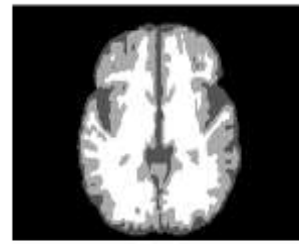
(b)

(c)

(d)

(e)

(f)

(g)

(h)

Fig.9 The segmentation results obtained by (a) CMRF, (b) PSO-MRF, (c) HMRF-EM,

(d) SPM, (e) PVC, (f) the proposed method along with (g) the original slice and (h) the

ground truth. Image: IBSR_01 slice128 (WM in white, GM in light gray, CSF in dark
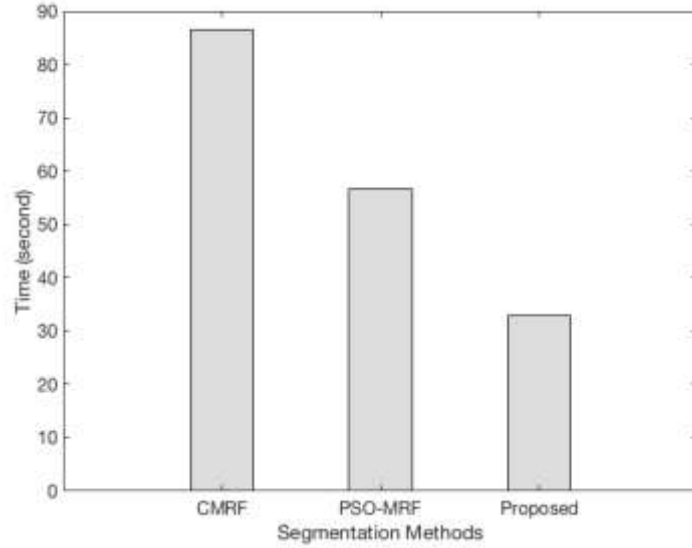
gray and the background in black).

Fig.10 Comparison of the mean computational time over each slice by the CMRF, the

PSO-MRF and the proposed method for the IBSR2.0 dataset.

Similar to Fig.5, Fig.10 shows the mean computational time of each slice by three

methods for the IBSR2.0 dataset, including the CMRF, the PSO-MRF and our proposed

method. For the real dataset, the proposed hybrid algorithm also consumes much less

time than the other two stochastic relaxation algorithms. The computational time

reduction percentages of our proposed method relative to the CMRF and the PSO-MRF

methods are 61.95% and 41.91%, respectively. The time reduction percentage indexes

for the IBSR2.0 dataset is comparable to that for the BrainWeb dataset, which shows that

compared to other stochastic relaxation algorithms, the proposed hybrid framework can

definitely save computational time for both the simulated and the real datasets.

4. Conclusions

This paper introduced a novel framework for brain MRI tissue segmentation. The motivation was that the RDPSO algorithm, as a global optimization method, can help achieve more accurate classification results when used within an MRF approach. Furthermore, we combined the RDPSO-MRF algorithm with the HMRF-EM approach to propose a hybrid framework, which can further improve the segmentation precision and speed up the convergence. There are two main reasons for the utilization of the HMRF-EM. First, the HMRF-EM method adopts the results obtained by the RDPSO-MRF algorithm to initialize its parameters, which can further be locally improved in terms of the segmentation performance. Second, as the RDPSO is a global stochastic algorithm, it does cost much computational time when performing optimization tasks, especially when coping with a large task like the optimization of the total energy of MRF, and we thus utilized the HMRF-EM framework to cut off some meaningless iterations in the running of the RDPSO-MRF. In contrast with two other traditional stochastic algorithms, the standalone HMRF-EM, and two widely used brain tissue segmentation toolboxes on both simulated and real MRI datasets, the proposed hybrid framework showed its advantages over all the other methods in terms of segmentation accuracy, and it converged to the optimal solutions much faster than the two compared stochastic algorithms.

In our future work, we will further improve the RDPSO algorithm with respect to its search ability and convergence speed, and take into account the bias field compensation in preprocessing in order to obtain better MRI segmentation results.

Acknowledgements

References

[1] Shanker R, Bhattacharya M. An automated Computer-Aided Diagnosis system for classification of MR images using texture features and Gbest- Guided Gravitational Search Algorithm. Biocyern Biomed Eng, 2020; 40:815-835.

[2] Sharma M, Bhattacharya M. Discrimination and quantification of live/dead rat brain cells using a non-linear segmentation model. Med Biol Eng Comput, 2020; 58:1127–1146.

[3] Cabezas M, Oliver A, Lladó X, Freixenet J, Cuadra M B. A review of atlas-based segmentation for magnetic resonance brain images. Comput Methods Programs Biomed 2011;104(3):e158–e177.

[4] Barker S, Rayner P J. Unsupervised image segmentation using Markov random field models. Pattern Recognit 2000;33(4):587–602.

[5] El-Dahshan E S A, Mohsen H M, Revett K, Salem A B M. Computer-aided diagnosis of human brain tumor through MRI: A survey and a new algorithm. Expert Syst Appl 2014;41(11):5526–

5545.

[6] Lao Z, Shen D, Liu D, Jawad A F, Melhem E R, Launer L J, Bryan R N, Davatzikos C. Computer-assisted segmentation of white matter lesions in 3D MR images using support vector machine. Acad Radiol 2008;15(3):300–313.

[7] Clarke L, Velthuizen R, Camacho M, Heine J, Vaidyanathan M, Hall L, Thatcher R, Silbiger M. MRI segmentation: methods and applications. Magn Reson Imaging 1995;13(3):343–368.

[8] de Boer R, Vrooman H A, Ikram M A, Vernooij M W, Breteler M M, van der Lugt A, Niessen W J. Accuracy and reproducibility study of automatic MRI brain tissue segmentation methods. NeuroImage 2010;51(3):1047–1056.

[9] Awate S P, Tasdizen T, Foster N, Whitaker R T. Adaptive Markov modeling for mutual-information-based, unsupervised MRI brain-tissue classification. Med Image Anal 2006;10(5):726–739.

[10] Ahmed M N, Yamany S M, Mohamed N, Farag A A, Moriarty T. A modified fuzzy c-means algorithm for bias field estimation and segmentation of MRI data. IEEE Trans Med Imaging 2002;21(3):193–199.

[11] Ahmadvand A, Daliri M R. Improving the runtime of MRF based method for MRI brain segmentation. Appl Math Comput 2015;256:808–818.

[12] Bhattacharya M, Chandana M. Analytical Assessment of Intelligent Segmentation Techniques for Cortical Tissues of MR Brain Images: A Comparative Study. Artif Intell Rev, 2012;37(1):69-81.

[13] Tutar I B, Pathak S D, Gong L, Cho P S, Wallner K, Kim Y. Semiautomatic 3-D prostate segmentation from TRUS images using spherical harmonics. IEEE Trans Med Imaging

2006;25(12):1645–1654.

[14] Lee J, Woo J, Xing F, Murano E Z, Stone M, Prince J L. Semi-automatic segmentation for 3D motion analysis of the tongue with dynamic MRI. Comput Med Imaging Graph 2014;38(8):714–724.

[15] Li S Z. Markov random field modeling in image analysis, Springer Science & Business Media, London: Springer, 2009.

[16] Zhang L, Ji Q. Image segmentation with a unified graphical model. IEEE Trans Pattern Anal Mach Intell 2010;32(8):1406–1425.

[17] Vaidya N M, Boyer K L. Discontinuity-preserving surface reconstruction using stochastic differential equations. Comput Vis Image Underst 1998;72(3):257–270.

[18] Arashloo S R, Kittler J. Fast pose invariant face recognition using super coupled multiresolution Markov Random Fields on a GPU. Pattern Recognit Lett 2014;48:49–59.

[19] Yang M, Liu Y, You Z, Li X, Zhang Y. A homography transform based higher-order MRF model for stereo matching. Pattern Recognit Lett 2014;40:66–71.

[20] Besag J. On the statistical analysis of dirty pictures. J R Stat Soc Series B Methodol 1986;48(3):259–302.

[21] Zerubia J, Chellappa R. Mean field annealing using compound Gauss-Markov random fields for edge detection and image estimation. IEEE Trans Neural Netw 1993;4(4):703–709.

[22] Bouman CA, Sauer K, Saquib S. Markov random fields and stochastic image models. 1995 IEEE International Conference on Image Processing, 1995;9.

[23] Dubes R, Jain A, Nadabar S, Chen C. MRF model-based algorithms for image segmentation. Proceedings in 10th International Conference on Pattern Recognition. IEEE, 1990;1:808–814.

[24] Tohka J, Dinov I D, Shattuck D W, Toga A W. Brain MRI tissue classification based on local Markov random fields. Magn Reson Imaging 2010;28(4):557–573.

[25] Cardoso M J, Clarkson M J, Ridgway G R, Modat M, Fox N C, Ourselin S, Initiative A N D. LoAd: a locally adaptive cortical segmentation algorithm. NeuroImage 2011;56(3):1386–1397.

[26] Yousefi S, Azmi R, Zahedi M. Brain tissue segmentation in MR images based on a hybrid of MRF and social algorithms. Med Image Anal 2012;16(4):840–848.

[27] Park S H, Lee S, Yun I D, Lee S U. Hierarchical MRF of globally consistent localized classifiers for 3D medical image segmentation. Pattern Recognit 2013;46(9):2408–2419.

[28] Sun J, Palade V, Cai Y, Fang W, Wu X. Biochemical systems identification by a random drift particle swarm optimization approach. BMC Bioinform 2014;15(S6):S1.

[29] Kennedy J, Eberhart R C. Particle swarm optimization. Proceedings of ICNN'95-International Conference on Neural Networks. IEEE, 1995;4:1942–1948.

[30] Shi Y, Eberhart R C. A modified particle swarm optimizer. 1998 IEEE international conference on evolutionary computation proceedings. IEEE world congress on computational intelligence (Cat. No. 98TH8360). IEEE, 1998:69-73.

[31] Solis F J, Wets R J B. Minimization by random search techniques. Math Oper Res 1981;6(1):19–30.

[32] Zhang Y, Brady M, Smith S. Segmentation of brain MR images through a hidden Markov random field model and the expectation-maximization algorithm. IEEE Trans Med Imaging 2001;20(1):45–57.

[33] Zhang T, Xia Y, Feng D D. Hidden Markov random field model based brain MR image segmentation using clonal selection algorithm and Markov chain Monte Carlo method. Biomed

Signal Process Control 2014;12:10–18.

[34] Guerrout E H, Mahiou R, Ait-Aoudia S. Hidden Markov random fields and swarm particles: A winning combination in image segmentation. IERI Procedia 2014;10:19–24.

[35] Bilmes J A. A gentle tutorial of the EM algorithm and its application to parameter estimation for Gaussian mixture and hidden Markov models. Int Comput Science Inst 1998;4(510):126.

[36] Geman S, Geman D. Stochastic relaxation, Gibbs distributions, and the Bayesian restoration of images. IEEE Trans Pattern Anal Mach Intell 1984;(6):721–741.

[37] Chellappa R, Jain A. Markov random fields. theory and application. Boston: Academic Press, 1993, edited by Chellappa, Rama; Jain, Anil, 1993.

[38] Hammersley J M, Clifford P. Markov fields on finite graphs and lattices. Unpublished manuscript, 1971.

[39] Liu X, Langer D L, Haider M A, Yang Y, Wernick M N, Yetik I S. Prostate cancer segmentation with simultaneous estimation of Markov random field parameters and class. IEEE Trans Med Imaging 2009;28(6):906–915.

[40] Held K, Kops E R, Krause B J, Wells W, Kikinis R, Muller-Gartner H W. Markov random field segmentation of brain MR images. IEEE Trans Med Imaging 1997;16(6):878–886.

[41] Han H, Li L, Duan C, Zhang H, Zhao Y, Liang Z. A unified EM approach to bladder wall segmentation with coupled level-set constraints. Med Image Anal 2013;17(8):1192–1205.

[42] Holzinger A, Blanchard D, Bloice M, Holzinger K, Palade V, Rabadan R. Darwin, lamarck, or baldwin: Applying evolutionary algorithms to machine learning techniques. 2014 IEEE/WIC/ACM International Joint Conferences on Web Intelligence (WI) and Intelligent Agent Technologies (IAT). IEEE, 2014;2:449–453.

[43] Holzinger K, Palade V, Rabadan R, Holzinger A. Darwin or lamarck? future challenges in evolutionary algorithms for knowledge discovery and data mining. Interactive Knowledge Discovery and Data Mining in Biomedical Informatics. Springer, Berlin, Heidelberg, 2014:35–56.

[44] Clerc M, Kennedy J. The particle swarm-explosion, stability and convergence in a multidimensional complex space. IEEE Trans Evol Comput 2002;6(2):58–73.

[45] Omar M A. Elementary solid state physics: principles and applications. Pearson Education India, 1975.

[46] Cardoso M J, Clarkson M J, Modat M, Ridgway G R, Ourselin S. Locally weighted Markov random fields for cortical segmentation. 2010 IEEE International Symposium on Biomedical Imaging: From Nano to Macro. IEEE, 2010:956–959.

[47] Van Leemput K, Bakkour A, Benner T, Wiggins G, Wald L L, Augustinack J, Dickerson B C, Golland P, Fischl B. Automated segmentation of hippocampal subfields from ultra-high resolution in vivo MRI. Hippocampus 2009;19(6):549–557.

[48] Rohlfing T, Brandt R, Menzel R, Maurer C R. Evaluation of atlas selection strategies for atlas-based image segmentation with application to confocal microscopy images of bee brains. NeuroImage 2004;21(4):1428–1442.

[49] Ashburner J, Friston K J. Unified segmentation. NeuroImage, 2005;26(3):839-851.

[50] Guo C, Ferreira D, Fink K, Westman E, Granberg T. Repeatability and reproducibility of FreeSurfer, FSL-SIENAX and SPM brain volumetric measurements and the effect of lesion filling in multiple sclerosis. Eur Radiol, 2019;29(3):1355-1364.

[51] Lindig T, Kotikalapudi R, Schweikardt D, Martin P, Bender F, Klose U, Ernemann U, Focke N

K, Bender B. Evaluation of multimodal segmentation based on 3D T1-, T2-and FLAIR-weighted images–the difficulty of choosing. NeuroImage, 2018;170:210-221.

[52] Shattuck D W, Sandor-Leahy S R, Schaper K A, Rottenberg D A, Leahy R M. Magnetic resonance image tissue classification using a partial volume model. NeuroImage, 2001;13(5):856-876.

[53] Valverde S, Oliver A, Cabezas M, Roura E, Lladó X. Comparison of 10 brain tissue segmentation methods using revisited IBSR annotations. J Magn Reson Imaging, 2015;41(1):93-101.

[54] Statistical Parametric Mapping (SPM) http://www.fil.ion.ucl.ac.uk/spm/

[55] BrainSuite Software http://neuroimage.usc.edu/neuro/BrainSuite/

[56] BrainWeb http://brainweb.bic.mni.mcgill.ca/brainweb/

[57] Internet Brain Segmentation Repository (IBSR) http://www.nitrc.org/projects/ibsr

[58] Rohlfing T. Image similarity and tissue overlaps as surrogates for image registration accuracy: Widely used but unreliable. IEEE Trans Med Imaging, 2012;31(2):153-163.